INTERNATIONAL ATOMIC ENERGY AGENCY
UNITED NATIONS EDUCATIONAL, SCIENTIFIC AND CULTURAL ORGANIZATION

INTERNATIONAL CENTRE FOR THEORETICAL PHYSICS
34100 TRIESTE (ITALY) - P.O.B. 586 - MIRAMARE - STRADA COSTIERA 11 - TELEPHONES: 224281/2/3/4/5/6
CABLE: CENTRATOM - TELEX 46392 ICTP

SMR-30/8

WINTER COLLEGE ON ATOMIC AND MOLECULAR PHYSICS

26 January - 18 March 1977

INTRODUCTION TO QUANTUM OPTICS: Part II
PHOTON STATISTICS

F.T. ARRECHI
Istituto Nazionale di Ottica
Firenze
and
C.I.S.E., Milano

2 - PHOTON STATISTICS

2.1 RELEVANCE OF PHOTON STATISTICS (PS)

Consider a photodetector illuminated by a light beam. By an electronic gate lasting for a time T, one counts the number n of photons annihilated at the photosurface in T. The random variable n has a statistical distribution p(n) that can be determined by iterating the above procedure for a large number of samples.

In Figure 2.1 we give an experimental plot of the statistical distribution of photocounts p(n) versus the number of counts

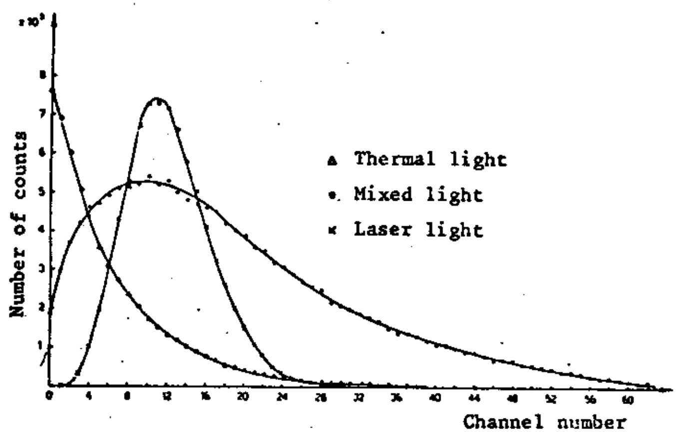

Fig. 2.1
Photocount distributions

$$n = \eta \langle I \rangle T$$

($\langle I \rangle$ being the average intensity, T the gating time , η a constant accounting for the quantum efficiency of the detector plus other instrumental factors). The three curves refer to three physical cases which are indistinguishable from the point of view of classical optics. Indeed in the three cases we have the same average photon number $\langle n \rangle$, the same diffraction limited plane wave, the same linewidth $\Delta\omega$ filtered out in such a way that

$$\tau_c = 1/\Delta\omega \gg T$$

that is, each sample of the statistical distribution p(n) is collected over a time T during which the field amplitude $|E|$ is practically constant. From the point of view of PS, the three lights are dramatically different as seen from the figure. The variances associated with distributions a) and b) are respectively :

$$\langle \Delta n^2 \rangle = \langle n \rangle$$

$$\langle \Delta n^2 \rangle = \langle n \rangle + \langle n \rangle^2$$

In the laser case p(n) is fitted by the familiar Poisson distribution which describes the number fluctuation in a volume containing a classical gas in equilibrium. The relative r.m.s. fluctuation is

$$\frac{\langle \Delta n^2 \rangle^{1/2}}{\langle n \rangle} = \frac{1}{\sqrt{\langle n \rangle}}$$

and for $\langle n \rangle \gg 1$ becomes negligible, justifying a description in terms of averages , as done in thermodynamics.

In the thermal case (light source in thermal equilibrium as for the black-body) the relative r.m.s. fluctuation does not decrease

$$\frac{\langle \Delta n^2 \rangle^{1/2}}{\langle n \rangle} \sim 1$$

hence, it is misleading to describe the field only in terms of average values $\langle n \rangle$.

The first contribution of (Δn^2) is a particle-like noise, as in the Poisson case [illegible] ; the second is a wave-like noise. If now one superposes a laser field with average photon number S and a thermal field with average $\langle n \rangle$ onto the same space mode, one obtains the sum of the two variances plus an interference term

$$\langle \Delta n^2 \rangle = S + \langle n \rangle + \langle n^2 \rangle + 2S \langle n \rangle$$

To show the importance of the last term consider a communication channel with S coherent photons and $\langle n \rangle$ noisy thermal photons. If e.g. $S = 10^4$, we get for the different $\langle n \rangle$ values :

$< n >$	$< \Delta n^2 >$
0	10^4
10	20×10^4

This shows the practical importance of these statistical considerations.

2.2 LIMITS OF CLASSICAL OPTICS

We show in this Section why the above questions are not accounted for in classical optics. We can expand the free field in a given region of space and time in orthonormal modes

$$\vec{E}(r,t) = \vec{E}^{(+)}(r,t) + \vec{E}^{(-)}(r,t)$$

$$= \sum_K [C_K \vec{u}_K(r) e^{-i\omega_K t} + C_K^* \vec{u}_K^*(r) e^{i\omega_K t}] \qquad (2.1)$$

where $E^{(+)}$, $E^{(-)}$ denote the positive and negative frequency parts of the Fourier expansion, and $u_K(r)$ can be calculated by suitable boundary conditions.

We express our ignorance on the sources of the field by saying that the complex field amplitudes C_K are random quantities assigned through a probability distribution

$$p(\{C_K\}) = p(C_1, C_2, \dots C_K, \dots) \qquad (2.2)$$

so that any field function is given in average by :

$$< f(E) > = \int f[E^{(+)}(\{C_K\})] \, p(\{C_K\}) \prod_K d^2C_K + c.c \qquad (2.3)$$

where :

$$d^2C_K = d(\mathrm{Re}\, C_K)\, d(\mathrm{Im}\, C_K)$$

We see therefore that a *complete* characterization of the field (2.1) implies knowledge of the joint probability of *all* the amplitudes C_K or, equivalently, of the correlation functions of the fields

$$G^{(n,m)} = < E^{(+)}(X_1) E^{(+)}(X_2) \dots E^{(+)}(X_n) E^{(-)}(X_{n+1}) \dots E^{(-)}(X_{n+m}) >$$

$$(X_i \equiv r_i, t_i) \qquad (2.4)$$

at any order (the ensemble average being performed as in (2.3)).

Directionality and monochromaticity, the properties associated with classical interferometers, give instead information on the *lowest order* correlation function, namely

$$G^{(1,1)} = < E^{(+)}(r_1\, t_1)\, E^{(-)}(r_2\, t_2) >$$

This can be shown with reference to the Young and Michelson interferometers (Figure 2.2 and 2.3).

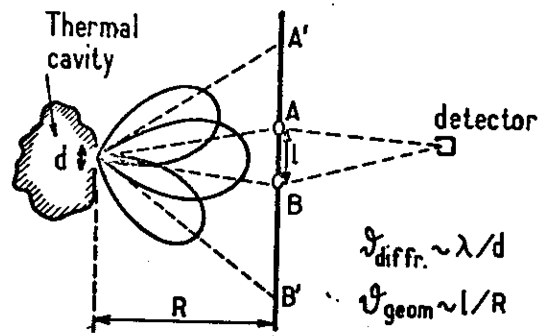

Fig. 2.2
Young interferometer and coherence area. To see fringes, geometrical angle l/R must be smaller than diffraction angle λ/d, hence (for solid angles) $l^2 < (R\,\lambda/d)^2 \equiv A$ (coherence)

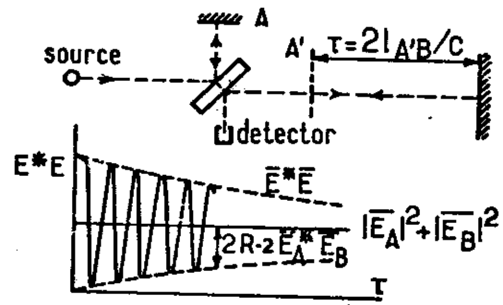

Fig. 2.3
Michelson interferometer and coherence time. To see fringes, τ must be smaller than the reciprocal of the source linewidth.

Let us consider a radiating cavity with an aperture d(Figure 2,2). In the expansion (2.1) inside that cavity each outgoing plane wave is broadened by diffraction by a solid angle $\theta_d^2 \sim (\lambda/d)^2$. In Figure 2.2 we sketch for each plane wave a polar diagram, centered at the center of the aperture, giving the distribution of the intensities around the central propagation vector k for three different plane waves. The Young interferometer is made of a screen with two diffraction holes A,B plus a square-law detector which time-averages the square of the instantaneous signal

$$\overline{| E_A + E_B |^2}$$

over a resolving time much longer than an optical period. As the detector moves parallel to the screen, it collects an average contribution $\overline{|E_A|^2} + \overline{|E_B|^2}$ (bar means time average) plus a cross-term contribution $2\mathrm{Re}\,\overline{E_A E_B}$ which can be either positive or negative depending on the phase relationship between E_A and E_B. This extra contribution gives rise to fringes.

If the source is in thermal equilibrium, we expect that the plane waves of the expansion (2.1) are mutually independent. Therefore the cross-term is non-zero only when the holes A,B pick up fields coming from the same diffracted plane wave, that is, fringes appear only when the distance between A and B is such that the geometrical aperture d/R is smaller than the diffraction aperture λ/d (Figure 2.2).

The fringes are an indication of selection of a single k (directionality).

Hence directionality is related to the quantity.

$$G^{(1,1)}(r_A,r_B) = \langle E^{(+)}(r_A,t)\, E^{(-)}(r_B,t) \rangle \qquad (2.5)$$

Similarly, in a Michelson interferometer (Figure 2.3) one investigates the monochromaticity of a source of bandwidth $\Delta\omega$ by introducing a delay

$$\tau = t_B - t_A$$

between the two mirrors B and A, and looking at the fringe decay as τ is increased. Here light is correlated at the *same space* point but at different times, and the cross term will be proportional to

$$\overline{E^{(+)}(r,t_A)E^{(-)}(r,t_B)} = \sum_{\Delta\omega} {}_{\ell m}\, \overline{C_\ell\, e^{-i\omega_\ell t}\, C_m^* \, e^{i\omega_m (t-\tau)}}$$

we have limited the sum over the linewidth $\Delta\omega$. Replacing the time average with an ensemble average, and using the assumed mode independence it results $\langle C_\ell C_m^* \rangle = |C_\ell|^2 \delta_{\ell m}$. Hence the sum reduces to

$$\sum_\ell |C_\ell|^2\, e^{-i\omega_\ell \tau} \sim |C_0|^2 \sum_{\Delta\omega} e^{-i\omega_\ell \tau}$$

and it gives a non-zero contribution only when the complex numbers

are almost phased, that is up to $\tau|\omega_\ell - \omega_{\ell'}| \lesssim 1$ or

$$\tau \sim 1/\Delta\omega$$

To conclude, the decay of fringes is associated with the decay of the term

$$G^{(1,1)}(t_A,t_B) = \langle E^{(+)}(r,t_A)\, E^{(-)}(r,t_B) \rangle \qquad (2.6)$$

In both cases, (2.5) and (2.6) give the number of k values or ω values within the resolution range of the interferometer, i.e. they show how to select a single mode from the mode expansion (2.1). We still have to solve the problem : how is each mode statistically distributed ? We must go over to higher order correlations as (2.4) with n,m > 1.

2.3 CHARACTERIZATION OF RANDOM PROCESSES.

A random process is described by a random function y(t) of time, which in realistic experiments we take as proceeding by quantized steps τ_R (τ_R = resolving time of the measuring set-up) and varying over a finite interval $(0,T_0)$. If we consider n values $t_1, t_2 \dots t_n$ of t in $(0,T_0)$, then the values $y(t_1), y(t_2) \dots y(t_n)$ are a set of random variables characterized by the hierarchy of joint probability distributions

$$W_1(y_1) \qquad (2.7)$$

(probability density of finding $y(t_1)$ between y_1 and $y_1 + dy_1$ normalized as

$$\int_{-\infty}^{\infty} W_1(y_1)\, dy_1 = 1)$$

$$W_2(y_1,y_2) \equiv W_1(y_1)\, P_c(y_1 | y_2) \qquad (2.8)$$

(joint probability of finding y_1 at t_1 and y_2 at t_2 ; this defines also a conditional probability of finding y_2 at t_2, given y_1 at t_1 through and so on. One should go up to W_n to fully characterize the process in $(0,T_0)$. However there are two simple random processes. The first is the fully random process in which no memory is kept of previous events, hence

$$W_n(y_1,y_2 \dots y_n) = W_1(y_1)\, W_1(y_2) \dots W_1(y_n)$$

The second is the Markoff process, completely characterized by W_2, in the sense that the conditional probability is with "short memory" as expressed by the self-explanatory relation

$$W_3(y_1\, y_2\, y_3) = W_2(y_1\, y_2) P_c(y_1\, y_2 | y_3) = W_2(y_1\, y_2)\, P_c(y_2 | y_3)$$

that is, P_c has no memory of y_1 but only of y_2.

An equivalent way of describing a random process is through the correlation functions

$$\langle y_1 y_2 \ldots y_n \rangle \equiv \int y_1 y_2 \ldots y_n \; W_n(y_1 y_2 y_n)\, dy_1\, dy_2 \ldots dy_n$$

for any set of times $(t_1 t_2 \ldots t_n)$ including repeated indices. When the random process is an electric field, of particular importance are the first two correlation functions,

$$G^{(1)}(1,2) \equiv \langle E_1^* \; E_2 \rangle \qquad (2.9)$$

which in particular for $t_1 = t_2$ becomes

$$I \equiv \langle E_1^* \; E_1 \rangle \qquad (2.9)^1$$

and

$$G^{(2)}(1,2) \equiv \langle I_1 \; I_2 \rangle = \langle E_1^* \, E_1 \, E_2^* \, E_2 \rangle \qquad (2.10)$$

The field correlation function was used in Sec. 2.2. The intensity correlation function will be used in Sec. 2.4.

2.4 GAUSSIAN PROCESSES AND THE HANBURY-BROWN AND TWISS EFFECT

Gaussian processes with zero average are those whose W_n are Gaussian :

$$W_1(y) = N\, e^{-y^2/\sigma^2}$$

and so on. An equivalent definition is by saying that the odd correlation functions are zero and the even ones factor out in all products of pairs :

$$\langle y_1 y_2 \cdots y_{2n+1} \rangle = 0$$

$$\langle y_1 y_2 \cdots y_{2n} \rangle = \sum_P \langle y_1 y_2 \rangle \langle y_3 \; y_4 \rangle \ldots \ldots \langle y_{2n-1} \; y_{2n} \rangle$$

where $\sum_P$ is sum over all permutations of (1.... 2n).

For example :

$$\begin{aligned} \langle y_1 y_2 y_3 y_4 \rangle &= \langle y_1 y_2 \rangle \langle y_3 \; y_4 \rangle \\ &+ \langle y_1 y_3 \rangle \langle y_2 \; y_4 \rangle \\ &+ \langle y_1 y_4 \rangle \langle y_2 \; y_3 \rangle \end{aligned} \qquad (2.11)$$

For a complex field, combining (2.10) and (2.11) one gets

$$\langle I_1 \; I_2 \rangle = \langle I_1 \rangle \langle I_2 \rangle + |\langle E_1^* \;\; E_2 \rangle|^2 \qquad (2.12)$$

This is a very important relation, showing that the Gaussian intensity correlation sheds information on the square of the field correlation (Figure 2.4).

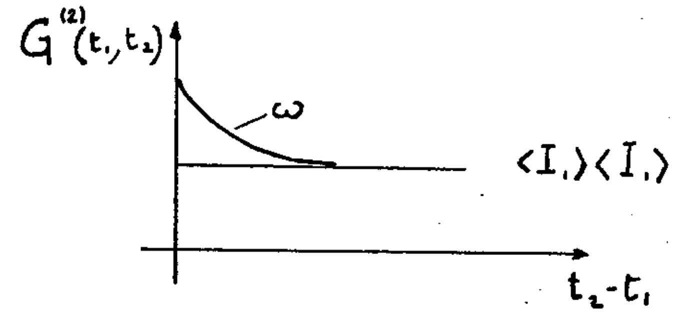

Figure 2.4:
Plot of the intensity correlation function.

Gaussian processes are important for two reasons.

A) Entropy argument

In a cavity at thermal equilibrium the entropy as a function of the variable E is a maximum S_0 ; hence expanding around S_0 one has

$$S(E) = S_0 - \alpha E^2$$

But the field probability is given by Boltzman relation

$$W(E) = e^{S/k} \to e^{S_0/k} \;\; e^{-(\alpha/k)E^2} ,$$

hence it is Gaussian

B) Central limit argument

By the central limit theorem, the sum of many uncorrelated events is Gaussian. Such is the case of light generated by the atomic spontaneous emissions in a thermal source, or the light scattered by microscopic bodies in a light scattering experiment. In such a case, the scattered field E_s is proportional to the impinging field E_0 and to the random polarizability $\Delta\varepsilon$ of the scattering medium :

$$E_s \propto \Delta\varepsilon . E_0$$

If E_0 is free from fluctuations (say, laser light) then the correlations in E_s repeat faithfully the correlations in $\Delta\varepsilon$ and hence give information on the medium behaviour. Eq. (2.4) says that the *intensity correlation* (as obtained with a photodetector plus an electronic correlator) gives *all* information on the scatterer (except for frequency shifts). Historically , all that was born by an extrapolation of the interferometer idea.

In 1956 it was introduced by Hanbury-Brown and Twiss a new interferometer correlating the outputs of two detectors, and therefore correlating the intensities rather than the fields (Figure 2.5).

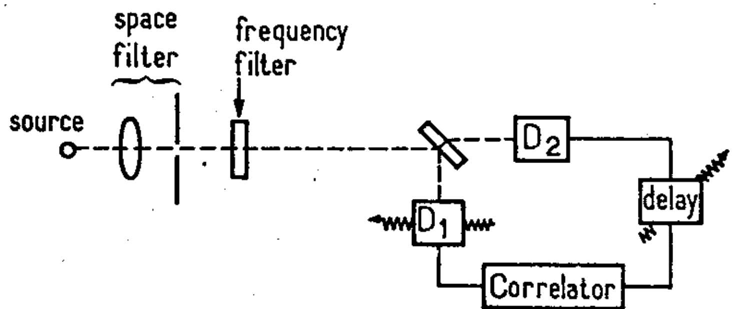

Fig. 2.5
Hanbury-Brown-Twiss interferometer D_I, D_2 detectors. Movement in D_I to pick up different angular regions ; variable delay between D_I and D_2 .

The outcome of the experiment is here proportional to :

$$G(2,2) = \langle |E_1|^2 \; |E_2|^2 \rangle$$

where E_1, E_2 are the fields at the two detectors. Suppose we have already selected by filters a single monochromatic plane wave :

$$E(r,t) = C\, e^{-i(\omega t - kr)} + C^* \, e^{i(\omega t - kr)}$$

Then (4.5) this time implies the statistical distribution of C, *not only* its average intensity, since it is proportional to the fourth moment :

$$\langle |C|^2 \; |C|^2 \rangle = \langle |C|^4 \rangle$$

Two typical examples are :

1. *Gaussian distribution with zero average :*

$$p(C) = \frac{1}{\pi\langle n \rangle} \; e^{-|C|^2/\langle n \rangle}$$

This corresponds to thermal equilibrium. Indeed it is a Boltzmann distribution $e^{-W/kT}/Z$ with $W = n\hbar\omega$ (n = photon number $\propto |C|^2$). It is well known that a complex Gaussian distribution has the following relation between fourth and second moment (see(2.12)):

$$\langle |C|^4 \rangle = 2 \langle |C|^2 \rangle$$

2. *"coherent" field without fluctuations :*

$$p(C) = \delta^{(2)}\,(C - C_0) \qquad (2.13)$$

($\delta^{(2)}$ is a Dirac δ -function in the complex plane G)

In such a case the intensity correlation is

$$\langle |C|^4 \rangle = \langle |C|^2 \rangle = |C_0|^4 \qquad (2.14)$$

Equations (2.13) and (2.14) suggest that coherence can be defined as : "δ-like amplitude distribution", or : "correlation functions factorized at any order".

The above equivalent definitions can be generalized to include a many-mode field. A field made of, say, two modes is coherent when :

$$p(C_1\,,\,C_2) = \delta^{(2)}\,(C_1 - C_{10})\;\delta^{(2)}\,(C_2 - C_{20}) \qquad (2.13)'$$

or

$$\langle E_1^{(+)} \; E_2^{(+)} \; .... \; E_{n+m}^{(-)} \rangle = \langle E_1^{(+)} \rangle \langle E_2^{(+)} \rangle \; ..... \langle E_{n+m}^{(-)} \rangle \qquad (2.14)'$$

but it may be neither monochromatic nor unidirectional !

2.5 MEASUREMENT OF THE PS

We give here a simple-minded picture based on the argument that photons being particles with zero mass cannot be localized when the field is uniform (Figure 6a).

Hence there are no a priori correlation between the outputs of two detectors 1 and 2, and the photons, whose average number is proportional to the square field and the measuring time T

$$\langle n \rangle = |E|^2 \, T \; \eta$$

(η = quantum efficiency of the detector)

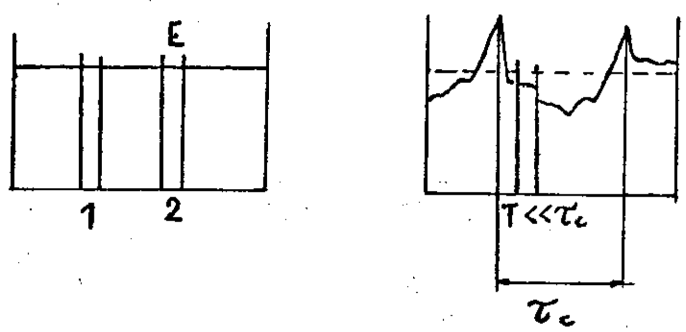

Figure 2.6:
Profile of the field amplitude for a coherent and a fluctuation field case. τ_c *= coherence time (decay time of the field correlation function) ; T = observation time.*

must be distributed as a Poissonian (as the statisticsof radioactive counts), that is :

$$p(n) = K(E, T\,|n) = \frac{\langle n\rangle}{n!}\, e^{-\langle n\rangle} \qquad (2.15)$$

If now (Figure 6 b) the field is randomly distributed with a statistics W_1 (E,t) and each measurement lasts for a time T much smaller than the coherence time τ_c ,

$$T \ll \tau_c \quad ,$$

... order to have a constant field within each sample, then we must average the detector statistics (5.1) over the field statistics

$$p(n, T,t) = \int K(E,T|\,n)\;\; W_1(E)\; dE$$

In Figure 2.7 the results are shown pictorially for the three cases of Figure 1.1.

The photodetector used in measurements is a high-gain low-noise multiplier phototube. Anode-current pulses corresponding to single photoelectrons are standardized in amplitude and shape by a nonlinear circuit. This way , we get rid of the amplitude fluctuations in the multiplication process on the dynodes. An integrating capacitor acts as a number to voltage converter, and its voltage suitably amplified is then classified by a multichannel pulse-height analyzer. An alternative way of counting the number of pulses in a given time interval T is to use a fast electronic scale, gated "on" for a time T, which records the number of pulses and is directly connected with the memory of the multichannel analyzer : this avoids the double conversion

process, thus increasing the rate at which counts can be accumulated.

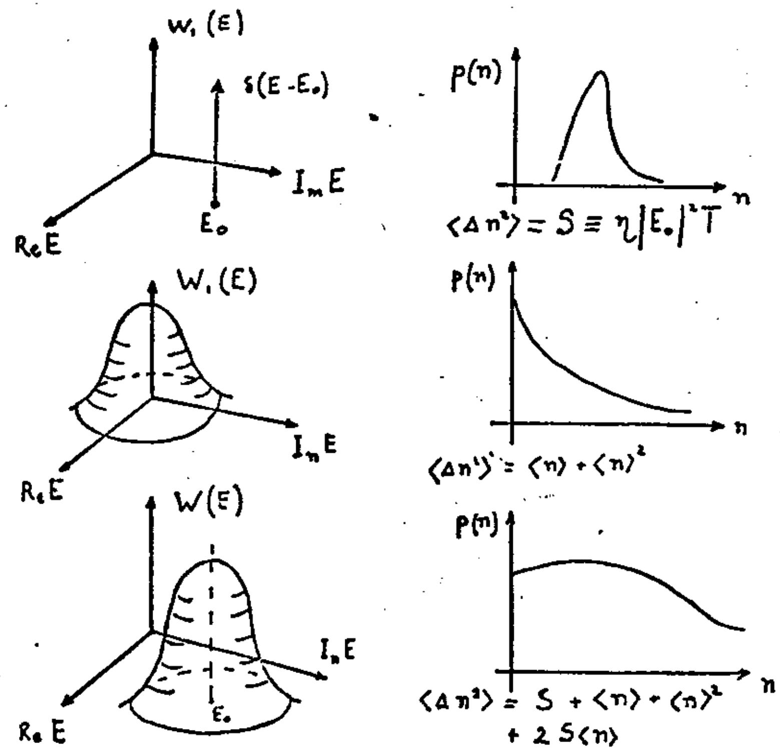

Figure 2.7:
Qualitative plot of the statistical distributions of field and photons for the three cases of Figure 1.

One obtains directly the distribution p(n,T) of photoelectron numbers. The distributions reported in Figure 1 have been obtained by this method.

A single p(n,T) gives only an integrated information on the time evolution of the field. One way of measuring the time evolution would be to measure the PS for increasing time-interval T up to (or larger than) the characteristic relaxation time of the field, and then to correlate the various shapes of the photocount distributions.

It is better however for the interpretation of the results to correlate separate observations, each one made for a time T much shorter than the the coherence time, as shown in the experimental set-up (Figure 2.8).

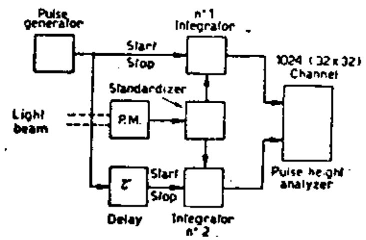

Figure 2.8:
Experimental setup used for measuring joint photocount distributions

Essentially, the operation described before is repeated twice at times t_1 and t_2 and the two results are sent to a two-dimensional multichannel pulse-height analyzer. The results are classified on a two-dimensional matrix, which gives the joint photocount distribution

$$W_2(n_1t_1,\ n_2t_2) = P_c(n_1t_1 \mid n_2t_2)\ W_1(n_1t_1')$$

One easily realizes that P_c is given by the reading on a row defined by the chosen value of n_1) (Figure 2.9) and it is symmetrical with respect to indices 1 and 2 for all stationary processes. The marginal distribution $W_1(n_1) = W_1(n_2)$ corresponding to an uncorrelated experiment of the kind described previously, is obtained by summing for each column (row) the values corresponding to all rows (columns) belonging to that column (row).

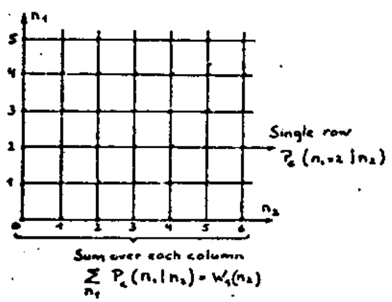

Figure 2.9:
Matrix of the output numbers (each represented by a dot) as they are printed at the digital output of the mutichannel analyser. The numbers on a given line (e.g the row n_1=2) give a conditional distribution.

In Figure 2.10 we give the experimental results for a stationary Gaussian field together with the theoretical curves.

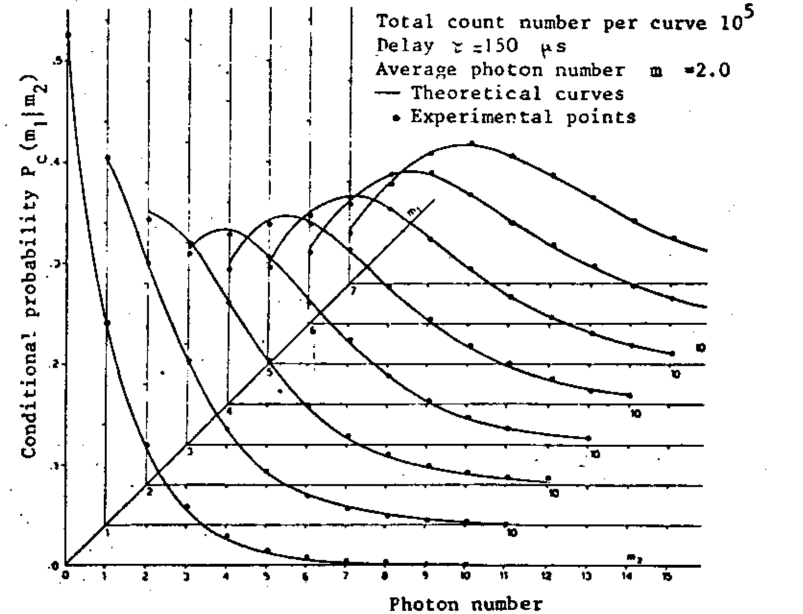

Figure 2.10:
Joint photocount distribution for a gaussian field (laser light scattered by a rotating ground glass disk) with a coherence time of 700 μsec. The delay is 150 μsec (Arecchi et al 1966 b).

2.6 LASER FLUCTUATIONS

A) A review of the theory

As an application of the PS we present a set of experiments on both the stationary and transient statistical properties of a laser system. Let us make a heuristic description of a laser.

First let us consider a damped harmonic oscillator. Its statistical amplitude can be described by means of a Langevin equation, which we write in a rotating frame, (that is, after a transformation $\alpha \to \alpha e^{-i\omega t}$) as

$$\dot{\alpha} + \gamma\alpha = \Gamma(t) \qquad (2.16)$$

Here $\alpha(t)$ is the complex amplitude of the oscillator, γ is the damping constant, and $\Gamma(t)$ is a random noise source. Let $\Gamma(t)$ be a complex stationary Gaussian process, with zero average and δ-correlated in time :

$$\langle \Gamma(t) \rangle = 0$$

$$\langle \Gamma^*(t) \quad \Gamma(0) \rangle = Q\, \delta(t)$$

In order to have the conditional probability $P(\alpha_0,0|\alpha,t)$ we must solve the two-dimensional Fokker-Plank equation associated with eq. (2.16) which is

$$\frac{\partial P}{\partial t} - \gamma \, \mathrm{div}_\alpha \, (\alpha P) = q \, \nabla^2_\alpha P$$

where $q = Q/4$. Its complete solution is (Figure 2.11).

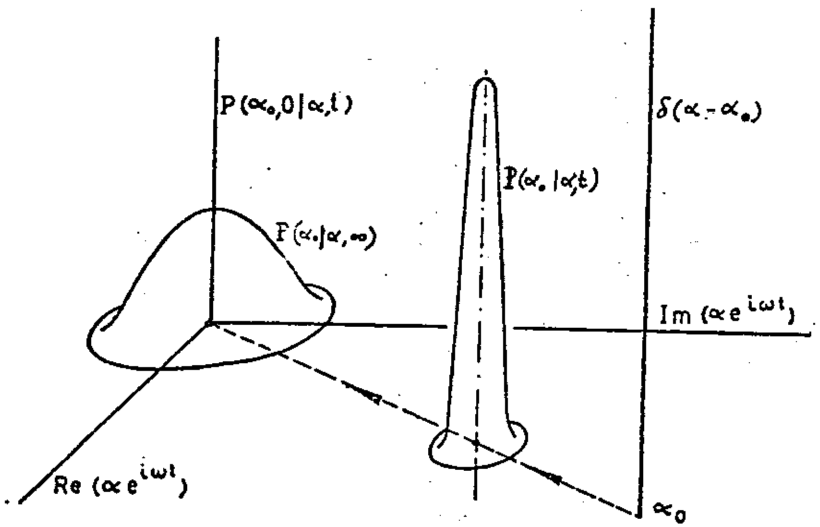

Figure 2.11:
Evolution of the conditional probability for a damped harmonic oscillator.

$$P(\alpha_0,0\,|\alpha,t) = \frac{1}{\pi\sigma^2(t)} \, e^{-\frac{|\alpha-\alpha_0 \exp(-\gamma t)|^2}{\sigma^2(t)}} \qquad (2.17)$$

where

$$\sigma^2(t) = \frac{2q}{\gamma}\,(1 - e^{-2\gamma t})$$

In the limit $t \to \infty$ we obtain the first-order probability density

$$\lim_{t\to\infty} P(\alpha_0 0|\alpha t) = W_1(\alpha) = \frac{1}{\pi 2q/\gamma} \, e^{-\frac{|\alpha|^2}{2q/\gamma}} \qquad (2.18)$$

By equation (2.17) the oscillator amplitude has been described as a stochastic Markoff process, whose ensemble distribution is a Gaussian with variance $\langle n \rangle = 2q/\gamma$ and whose frequency spectrum is Lorentzian with half-width $\Delta\omega = \gamma$ (i.e whose first-order correlation function has an experimental time decay with time constant $1/\gamma$).

We may apply this treatment to a single-mode laser field and think of it as an oscillator whose damping is compensated by a gain term G due to the excited atoms in the cavity. The associated Langevin equation is

$$\dot{\alpha} + (\gamma - G)\,\alpha = \Gamma(t)$$

Generally G is amplitude dependent, but in first approximation it can be considered as a constant $G=g_0$. In this case the same solution (2.17), (2.18) still hold, in which we have simply to replace γ with $\gamma - \gamma g_0$. A more realistic picture is obtained considering the dependence of G on $|\alpha|^2$ (cubic nonlinearity in the induced dipole moment), that is

$$G = g_0 - \beta \, |\alpha|^2$$

The Langevin equation becomes

$$\dot{\alpha} - \beta(d - |\alpha|^2)\alpha = \Gamma(t) \qquad (2.16)$$

where the linear negative damping $\beta d = g_0 - \gamma$ comes from the linear theory and $\beta|\alpha|^2$ is the first nonlinear correction. The Fokker-Plank equation becomes more complicated and we give only the final results. Its stationary solution in the plane $\alpha \equiv re^{i\phi}$ is independent of ϕ and is given by :

$$P(r) = Ne^{-\frac{\beta}{4q} r^4 + \frac{\beta d}{2q} r^2} \qquad (2.18)$$

It is suitable to introduce the pumping parameter

$$a = \sqrt{\frac{\beta}{q}}\; d \qquad (2.19)$$

and to normalize the square modulus as $X^2 = \sqrt{\frac{\beta}{q}}\, r^2$. The P(r) distribution is then written as

$$P(X) = Ne^{-\frac{1}{4}X^4 + \frac{a}{2}X^2} \qquad (2.20)$$

We define the threshold point as $\gamma = g_0$, that is, as that point where the linear gain is equal to the losses. At threshold

$$d = a = 0$$

Below threshold $(a < 0)$, the distribution (2.20) has a peak at $x=0$, whilst above threshold $(a > 0)$ it exhibits a peak at $X = \sqrt{a}$. It is easily shown that, outside the interval around threshold, the following approximation hold :

1) Far below threshold ($a < -10$). Equation (2.20) reduces to :

$$P(r) \sim Ne^{-\frac{|a|}{2} X^2} = N e^{-\frac{\beta|d|}{2q} r^2}$$

which is a Gaussian distribution centered at $r=0$, with a variance $< X^2 >$ equal to $2/|a|$ (Figure 14) for $a<0$).

2) Far above threshold ($a > 10$) .

The saturation becomes strong and tends to stabilize the field amplitude around its average value $< x> = \sqrt{a}$

The field statistics is

$$p(X) = N' e^{-a(X-\sqrt{a})^2} \qquad (2.20)'$$

This is a Gaussian distribution centered at $x = \sqrt{a}$.
P(x) as given in equation (2.20)' is only a modulus distribution uniform in phase.

We give now the time evolution of the field in the same two limiting cases.

1) Far below threshold. The following formulas hold for the field and intensity correlation functions respectively :

$$G^{(1)}(\tau) = < \alpha^*(\tau) \ \alpha(0) > = \frac{2q}{\beta|d|} e^{-\beta|d|\tau}$$

$$G^{(2)}(\tau) = <|\alpha(\tau)|^2|\alpha(0)^2|> + \left(\frac{2q}{\beta|d|}\right)^2 e^{-2\beta|d|\tau}$$

The Fourier transforms of these expressions give the spectra of the field and intensity fluctuations. These spectra have Lorentzian shapes, half-widths $\lambda^{(1)} = \beta|d|$, $\lambda^{(2)} = 2\lambda^{(1)}$ respectively.

These behaviour are illustrated in Figures 12 and 13 for $a < 0$.

2) Far above threshold.

Far above threshold the field distribution is peaked at $\sqrt{d}$.

The laser field appears as the linear superposition of a coherent field with amplitude $\sqrt{d}$ plus a Gaussian field with zero average, photon number given by :

$$< n > = \frac{q}{2\beta d}$$

and decay constant increasing linearly with d, that is

$$\Delta\omega = 2\beta d$$

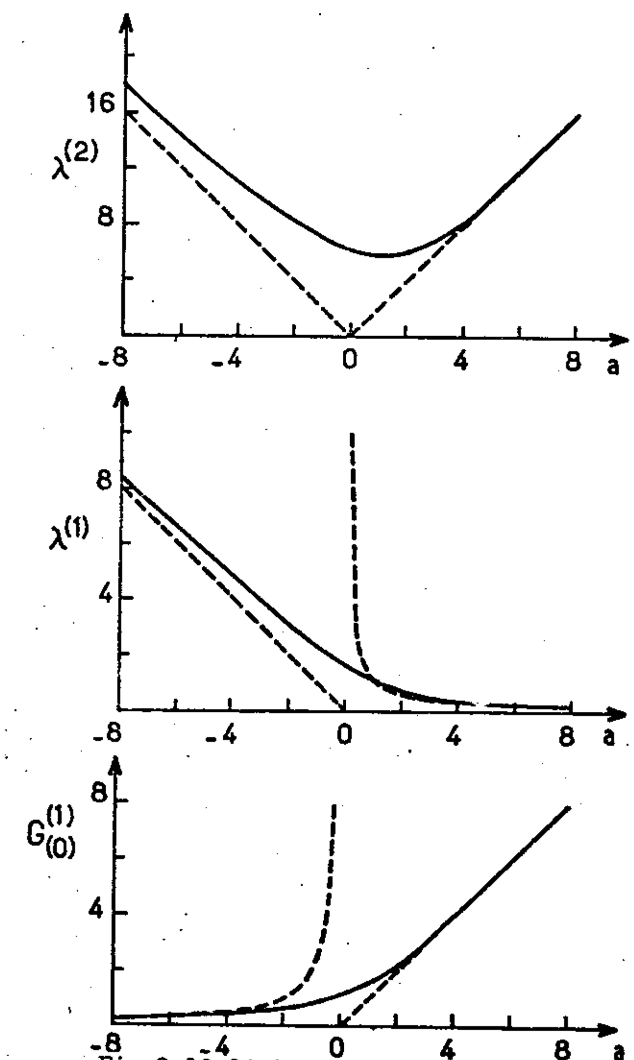

Fig.2.12-13-14 :
Decay constants $\lambda^{(2)}$ of $G^{(2)}(t)$ and $\lambda^{(I)}$ of $G^{(I)}$, and intensity $G^{(I)}(0)$, versus pump parameter a. Dashed lines : linearized theory. Solid lines : exact solution of Fokker-Planck equation.

As for the phase ϕ, it obeys a diffusion equation, whose solution has a diffusion constant q/d proportional to the reciprocal of the output power (Townes formula for a maser oscillator) ; see Figure 2.13 for $a > 0$.

3) Laser at threshold

So far we have discussed only the cases well above and below threshold. The behaviour in the threshold region cannot be obtained by simple extrapolation of the previous results, and we need a complete solution.

We refer to the theoretical calculations by Risken .[14] His solutions are plotted as solid lines in Figure 2.12 to 2.14 and are again reported for comparison in the experimental results (Figures 2.15 to 18). We see that the threshold point does not show discontinuities as it should appear from a naive linear picture.

B) Stationary experiments (ensemble distributions and time correlation). [12, 13]

In this Subsection we describe the experimental results obtained by means of the PS method in the study of the statistics of the e.m.field of a stabilized laser operating in different conditions. We used a 6328 Å He-Ne laser, single TEM_{00} mode, with one mirror supported by a piezoceramic disc in order to stabilize against fluctuations and to move the mode position with respect to the atomic line.

The measurement of p(n) is performed as described above. For comparing experiments and theory we used the second reduced factorial moment of the photocount distribution

$$H_2 = \frac{\langle n\,(n-1)\rangle}{\langle n\rangle^2} - 1 \qquad (2.21)$$

which goes from 1 (Gaussian field distribution ; well below threshold) to 0 for an amplitude-stabilized field (well above threshold), and the third one

$$H_3 = \frac{\langle n\,(n-1)\,(n-2)\rangle}{\langle n\rangle^3} - 1$$

which goes from 5 (Gaussian distribution) to 0 (amplitude- stabilized field) (Figure 2.15 and 2.16).

From the stationary solution of the Fokker-Planck equation for the statistical distribution of the laser field one can derive the distribution of photocounts and the associated factorial moments. One can see from the figures that the agreement between experiments and theory is very good. Finally we report the frequency spectra of the intensity fluctuations, and show that they are consistent with the time dependent solutions of the same Fokker-Planck equation, whose stationary solution is fitted by the ensemble distribution reported above.

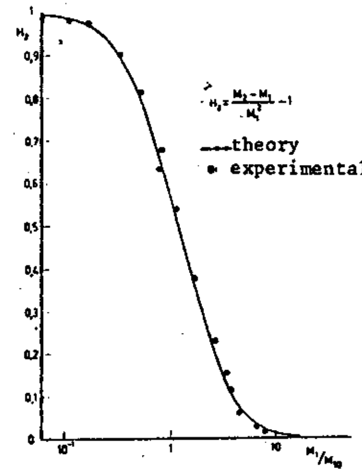

Figure 2.15:
Measured and theoretical values of the reduced second-order factorial moment H_2 as a function of the normalized intensity M_I/M_{IO} in the threshold region.—Theory, • Experimental point.

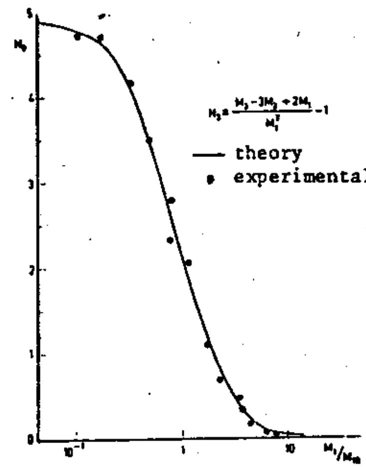

Figure 2.16:
Measured and theoretical values of the reduced third-order factorial moment H_3 as a function of the normalized intensity M_I/M_{IO} in the threshold region.—Theory, • experimental point..

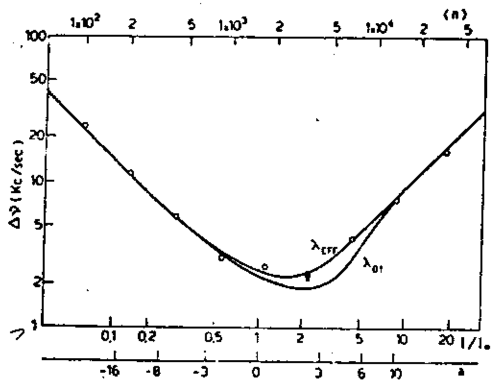

Figure 2.17:
Plot of the "effective "linewidth $\Delta\nu$ vs the laser intensity I normalized to the threshold values I_0 . The horizontal axis is also calibrated in values of the pump parameter a and in average photon number $<n>$ inside the cavity.

The results are reported in Figure 2.18 and 2.19.

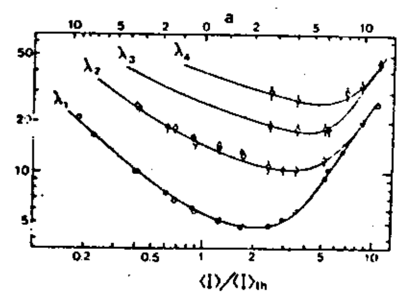

Figure 2.18
Plots of the relaxation rates of the laser intensity fluctuations. The full curves represent the theoretically predicted results. The standard deviations for the experimental points are reported only when they exceed the dot size. The two values of the proportionality constant C are $0,97 \times 10^3$ (open dots) and $1,03 \times 10^3$ (full dots).

The power spectra of the intensity fluctuations measured with a wave analyzer showed small deviations from a Lorentzian shape in the threshold region. For any spectral shape, we define the "effective" linewidth $\Delta\nu$ of an equivalent Lorentzian as the ratio between

the total spectral power and the zero frequency value of the spectral density.

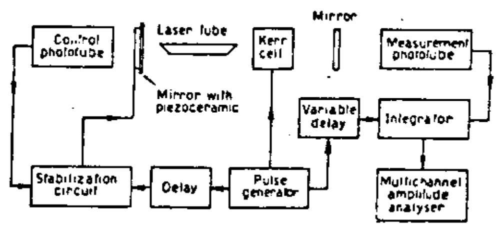

Figure 2.19:
Experimental set-up for the transient experiment.

The measured linewidth fits the numerical calculations of Risken and Vollmer [14] who gave a dynamical solution for the intensity correlation function as a sum of several exponential terms (with decay constants $\lambda_k^{(2)}$) occuring with weights M_k. This leads to an equivalent decay constant.

$$\lambda_{eff}^{(2)} = \left(\sum_k \frac{M_k}{\lambda_k^{(2)}} \right)^{-1} \qquad \sum_k M_k = 1$$

In the Figure 2.18 we have also plotted the main decay constant of the intensity correlation function. It is clear that a Lorentzian approximation with a single decay constant is not an adequate description.

By using a correlator rather than a frequency analyzer it has been recently possible to measure the first four decay constant versus the laser intensity (Figure 2.18). [13 bis]

C) Transient experiments [15]

By joint use of a Q-switched gas laser and of the linear method for PS one can study a nonstationary statistical ensemble, measuring the time evolution of a laser field during a fast built-up.

The experimental set-up is shown in Figure 2.19. We put a Kerr cell with end faces at the Brewster angle within a single mode 6328Å He-Ne laser cavity.

Starting with some pre-set pump and cavity-parameters, but with the optical shutter closed, the Kerr cell is switched "on" in a time shorter than 5 ns at the instant t=0. The laser field undergoes a transient build-up, from an initial statistical distribution corresponding to the equilibrium between gain and losses far below threshold up to an asymptotic condition above threshold. At the instant $t=\tau$ we perform photocount measurements for a measuring interval T of 50 ns, very small compared to the build-up time which is in our case of the order of some microseconds. Once a steady-state condition has been reached, an amplitude-stabilizing operation is performed by sampling the laser output and comparing this with a standard reference signal. This is equivalent to "preparing" an identical initial state for a successive measuring cycle.

After the sampling, the shutter is switched off for about 10ms. At the end of this interval the shutter is again switched on and the above described cycle of operations is repeated. This way, we collect an ensemble of macroscopically identical events. By varying successively τ, we obtain the time evolution of the photocount distribution $p(n,T,)$.

A set of experimental results is shown in Figure 2.20.

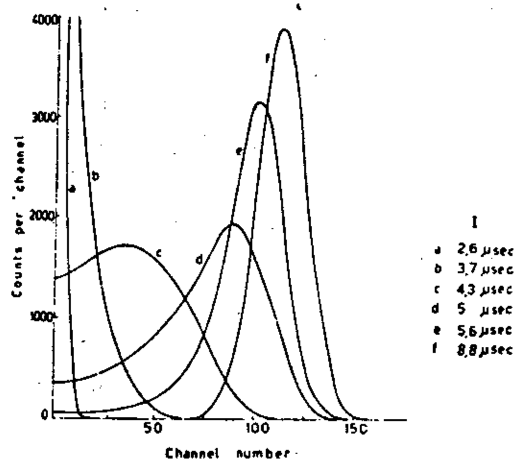

__Figure 2.20 :__
Experimental statistical distribution with different time delays obtained on a laser transient. The solid lines connect the experimental points which are not shown to make clearer the figure. All distributions are normalized to the same area a) 2.6μs; b) 3.7 μs; c) 4.3 μs; d) 5 μs; e) 5.6 μs; f) 8.8 μs.

The average photocount number $\langle n \rangle$ and the associated variance $\langle \Delta n^2 \rangle = \langle n^2 \rangle - \langle n \rangle^2$ are reported as function of the time delay in Figure 2.21 and 2.22 for two different pumping conditions.

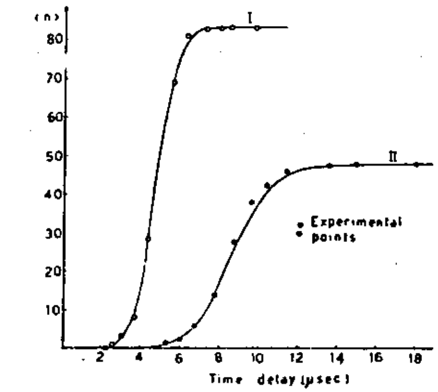

__Figure 2.21 :__
Evolution of the mean value $\langle n \rangle$ of the statistical distribution $p(n,T,\tau)$. The solid lines represent the theoretical curves which best fit the experimental points(∘,•).The experimental moints related to curve I) have been obtained by the statistical distribution of Fig 2.20.

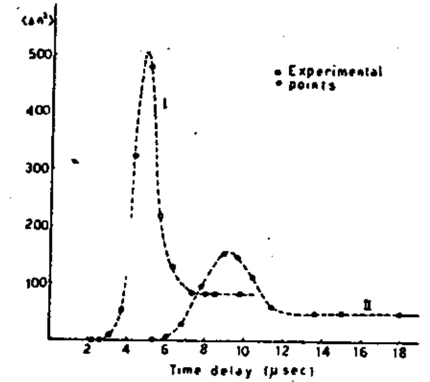

__Figure 2.22:__
Evolution of the variance $\langle \Delta n^2 \rangle = \langle n^2 \rangle - \langle n \rangle^2$ of the statistical distribution $p(n,T,\tau)$ Dashed lines represent an interpolation of the experimental points (∘,•).

Notice that in Figure 2.22 the dashed line just interpolates the experimental points but has no theoretical significance. In Figure 2.23 we correct for attenuation, as described in the next Section, and we see that the experimental points agree with the theoretical, solid line.

2.7 DISTORTION OF PS DUE TO ATTENUATION. [18]

The role of attenuation (Figure 24) is as follows.

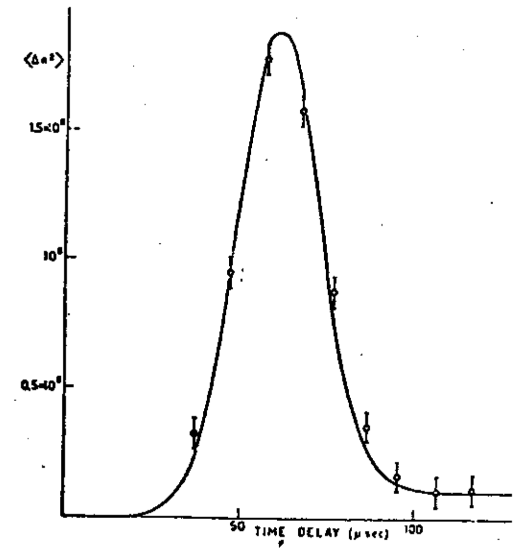

Figure 2.23:
Evolution of the variance $\langle \Delta n^2 \rangle$ of the statistical distribution of photons inside the laser cavity, as a function of the time delay τ. The solid line represents theoretical results (Arrecchi and Degiorgio 1971).

For a n-photon field (as described in quantum mechanical books) the attenuation would give rise to a binomial statistics as the partition noise through the grid of an electron vacuum tube. However for a statistical mixture of coherent fields (each having a Poisson spread in photon number as described above) the attenuation is a purely classical process

$$E' = \eta E$$

which affects the statistics leaving unaffected the elementary probability

$$P(E')\, d^2E' = P(E)\, d^2E \tag{2.22}$$

By use of (2.22) it is easily shown that the factorial moments, given by :

$$F_k \; \langle n(n-1)\ldots(n-k+1)\rangle = \int |E|^{2k} P(E)\, d^2E$$

change as

$$F'_k = \eta^{2k} F_k \tag{2.23}$$

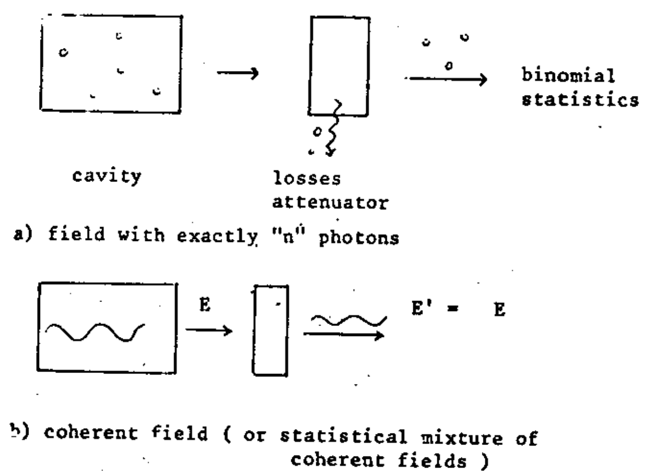

Figure 2.24:
Picture of "particle-like" and "wave-like" attenuation.

By (2.23) one can perform corrections for an attenuation η. This kind of correction has led from Figures 22 to 23.

2.8. THE PHOTOMULTIPLIER AS A STATISTICAL DEVICE.

The finite response time of the photodetector puts a limit on the use of PS for short times. We show here how intensity correlations can be corrected for the detector resolution. The output i(t) of a photocathode illuminated by a light signal may be represented by a train of photo-electrons localized at random times t_k, that is,

$$i(t) = \sum_{k=1} \delta(t - t_k)$$

The first correlation function $R_i(\tau) = \langle i(t)\, i(t+\tau) \rangle$ of the random process $i(t)$ which we assume stationary, is given by :

$$R_i(\tau) = \langle \sum_k \sum_j \delta(t-t_k)\, \delta(t+\tau-t_j) \rangle$$

$$= \langle \sum_k \delta(t-t_k)\, \delta(t+\tau-t_k) \rangle + \langle \sum_{k\neq j} \sum_j \delta(t-t_k)\, \delta(t+\tau-t_j) \rangle \qquad (2.24)$$

$$= \mu\delta(\tau) + \mu^2 g^{(2)}(\tau),$$

where μ is the average rate of photo-electrons, which is proportional to the average light intensity, and $g^{(2)}(\tau)$ is the reduced intensity correlation function.

The photomultiplier, considered as a linear stochastic filter (see Ref. [19]) is described by a random response function $h(t)$ which is the output for a single photo-electron emitted at time $t=0$. Consequently the random output current $u(t)$ will be the time convolution of the two random functions $h(t)$ and $i(t)$, that is,

$$u(t) = \int_{\infty}^{\infty} i(t-t')\, h(t')\, dt' \equiv i(t) * h(t)$$

In performing this convolution one should remember that the different $\delta(t-t_k)$ of the input are associated with independent realizations $h_{(k)}(t)$ of the random process $h(t)$. The correlation function $R_u(\tau) = \langle u(t)\, u(t+\tau) \rangle$ is computed by taking into account that the statistical properties of the photomultiplier operating in the linear range are independent from the statistics of $i(t)$ and that $h_{(k)}$ and $h_{(j)}$ for $k \neq j$ are statistically independent samples. It reads

$$R_u(\tau) = \mu^2\, g^{(2)}(\tau) * G(\tau) + \mu C(\tau) \qquad (2.25)$$

where : $$G(\tau) = \int_{\infty}^{\infty} \langle h(t) \rangle \langle h(t+\tau) \rangle\, dt$$

and $$C(\tau) = \int_{\infty}^{\infty} \langle h(t)\, h(t+\tau) \rangle\, dt$$

A full description of the effect of the photomultiplier on the intensity correlation function $R_u(\tau)$ requires therefore two different functions $C(\tau)$ and $G(\tau)$. $C(\tau)$ modifies the δ-like term of Equation (2.24), which comes from the discrete character of the detection process, whereas $G(\tau)$ modifies the term describing the joint probability of two different photon events.

The fluctuations of $h(t)$ are mostly generated by three effects : gain statistics at the dynodes, spread in transit times of secondary electrons from dynode to dynode, spread in the transit time of photoelectrons from the photocathode to the first dynode. If only the

first effects were present, $C(\tau)$ would be proportional to $G(\tau)$, whereas spreads in transit times affect the two functions differently. In particular, the spread associated with the transit time of photoelectrons affects only the location of each $h(t)$ and hence does not affect $C(\tau)$. As an example, we report in Figure 2.25 experimental results on both $C(\tau)$ and $G(\tau)$ (see Ref [19] and Ch. A5 of laser Hand-book). The two functions in Figure 2.25 are normalized to the same initial value.

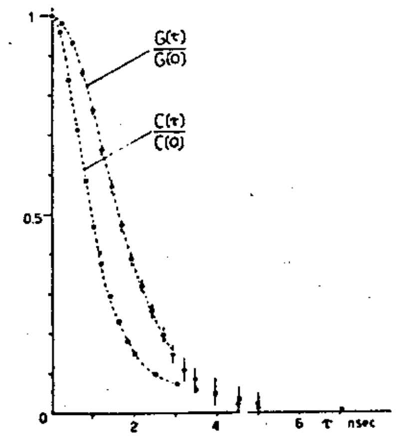

Figure 2.25

Plot of the functions $C(\tau)$ and $G(\tau)$ for a philips XP I2I0 photomultiplier, operating at 3800 V. The dashed lines interpolate the experimental points (Arecchi et Al I97I).

To obtain information on the light intensity correlation $g^{(2)}(\tau)$ from the measured correlation $R_u(\tau)$, the term $\mu C(\tau)$ must be subtracted. In this correction experimental errors strongly affect the results, especially at low photon flux. However the term $\mu C(\tau)$ does not appear at all in the expression for $R_u(\tau)$ when the correlation is performed with two phototubes. In that case, a similar calculation leads to a modified form of Equation (2.25)

$$R_u(\tau) = \langle u_1(t)\, u_2(t+\tau) \rangle = \mu_1\mu_2\, g^2(\tau) * G_{12}(\tau) \qquad (2.26)$$

where the indices 1 and 2 refer to the two phototubes and

$$G_{12}(\tau) = \int_{-\infty}^{\infty} \langle h_1(t) \rangle \langle h_2(t+\tau) \rangle\, dt$$

The treatment can be easily generalized to the measurement of higher-order correlation functions.

- REFERENCES

[1] R.J. Glauber : in *Quantum Optics and Electronics* (Proceedings of Les Houches 1964 Summer School) ed. by C.De Witt, et al. (New York 1965) plus previous references reported therein.

[2] R.J. Glauber : in Physics of Quantum Electronics (Proceedings of 1965 Puerto Rico Conference), ed. by P. Kelley, et al. (New York 1966).

[3] L. Mandel and E. Wolf : Rev. Mod. Phys. ,37, 213 (1965).

[4] M.C. Wang and G.E. Uhlenbeck : Rev. Mod. Phys.,17, 323 (1945).

[5] F.T. Arecchi : in Quantum Optics ed. by R.J. Glauber (1967 E. Fermi School)Academic Press.

[6] F.T. Arecchi : Phys. Rev. Lett. 15 , 912 (1965)

[7] F.T. Arecchi , A. Berné and P. Burlamacchi : Phys. Rev. Lett.16 ,32 (1966)

[8] F.T. Arecchi, A. Berné and A. Sona : Phys. Rev. Lett., 17 ,260 (1966)

[9] F.T. Arecchi , A. Berné, A. Sona and P. Burlamacchi: Proc of the IV International Quantum Electronics Conference, Phoenix 1966; IEEE Journ. Quantum Electronics, 2 , 341 (1966).

[10] F.T. Arecchi, E. Gatti and A. Sona : Phys. Lett. 20, 27 (1966)

[11] H. Risken : Zeits Phys.,186, 85 1965 ; 191 302 1966.

[12] F.T. Arecchi, G.S. Rodari and A. Sona :Phys.Lett. 25A ,59 1967.

[13] F.T. Arecchi, M. Giglio and A. Sona :Phys.Lett.25A ,341 1967.

[13] (Bis) M. Corti ,V. Degiorgio and F.T. Arecchi :Optics Commun, 8 329 (1973)

[14] H. Risken and H.D. Vollmer: Zeits.Phys. 201 ,323 (1967)

[15] F.T. Arecchi, V. Degiorgio and B. Querzola: Phys. Rev.Lett,19 ,1168 (1967); Arecchi-Degiorgio, Phys. Rev. A3 ,1108 (1971).

[16] W.E. Lamb: Phys.Rev. 134, A 1429 (1964)

[17] F.T. Arecchi ; M. Giglio and U. Tartari: Phys. Rev.163 (1967).

[18] F.T. Arecchi ,V. Degiorgio:Phys.Letters 27A ,429 (1968)

[19] F.T. Arecchi, M. Corti, V.Degiorgio, S.Donati :Opt. Comm.3, 284(1971)

Note : For a more up to date reference on Photon statistics and Laser fluctuations see Part A of

Laser Handbook (F.T. Arecchi, E.O. Schultz Du Bois eds). North Holland 1972.